Optical Particle Sizing in Backscatter

by

N. Damaschke[(1)] , H. Nobach[(2)], N. Semidetnov[(3)], C. Tropea[(4)]

Darmstadt University of Technology
Chair of Fluid Mechanics and Aerodynamics
Petersenstr. 30, 64287 Darmstadt, Germany

[(1)]e-mail: nils.damaschke@sla.tu-darmstadt.de
[(2)]e-mail: holger.nobach@nambis.de
[(3)]e-mail: nikolay@sla.tu-darmstadt.de
[(4)]e-mail: ctropea@sla.tu-darmstadt.de

ABSTRACT

Several possibilities of using elastic light scattering in the backscatter range (scattering angle $\vartheta_S > 140$ deg) for determining size, velocity and refractive index of spherical particles are investigated. First the phase Doppler technique is considered. Numerical simulations of the light scattering using the Lorenz-Mie theory (LMT) are used to show that the phase Doppler technique is unsuitable for such backscatter configurations, except for very special measurement conditions. The time-shift (or pulse displacement) technique is considered for sizing particles using elastic light scattering in the backscatter direction. Simulations using the Fourier Lorenz-Mie theory (FLMT) show that up to four fractional signals can be obtained using this technique in backscatter, corresponding to the scattering order/modes: surface wave (long path), reflection, second-order refraction (inner path), and a mixture of second-order refraction (outer path) and surface wave (short path). The situation for the backscatter range is illustrated in Fig. 1, in which a one-dimensional Gaussian intensity distribution is shown for a single incident beam. A particle moving through the beam in the scattering plane will result in various fractional signals arriving sequentially at the detector, hence the name time-shift technique.
Signal characteristics as a function of particle size, refractive index and particle ellipticity are studied. Suggestions for a practical measurement instrument are put forward.

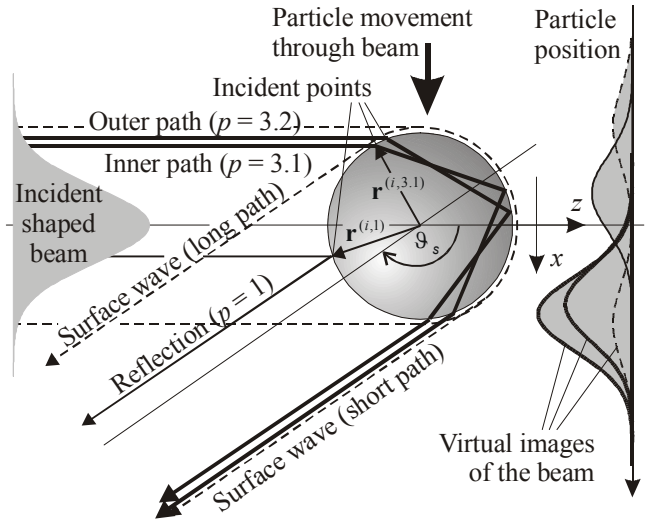

Fig. 1. Scattering orders/modes contributing to the signal in the near backscatter region for $m > 1$

1. INTRODUCTION

One major disadvantage of the phase Doppler technique for sizing is the restricted range of scattering angles at which the receiving optics can be placed relative to the transmitting optics. The permissible angular range is dictated primarily by the relative refractive index m (particle to surrounding medium) and the scattering order used, e.g. reflection or first-order refraction. A linear relationship between the measured phase difference and the particle diameter exists only when a single scattering mode dominates. Typical scattering angles ϑ_s for droplets ($1.2 < m < 1.5$) are in the range $20\,\text{deg} < \vartheta_s < 80\,\text{deg}$ (first-order refraction $p = 2$) and for bubbles ($m = 0.75$) in the range $90\,\text{deg} < \vartheta_s < 110\,\text{deg}$ (reflection $p = 1$). For applications this means that two optical accesses to the measurement point are necessary, one for the incident light beams and one for the scattered light. This can represent a difficult and costly requirement in many cases. Particle sizing in backscatter $\vartheta_s > 145\,\text{deg}$ would be much more convenient, allowing the incident and scattered light to pass through a single optical access. However, such a backscatter configuration of the phase Doppler technique is not be possible while maintaining a high single scattering order dominance.

Some mixture of scattering orders would have to be tolerated, which then degrades the linearity of the diameter/phase difference conversion factor, hence the measurement accuracy. Despite this fact, several attempts at realizing a backscatter phase Doppler instrument have been made. Bultynck (1998) has examined the feasibility of three possible arrangements exploiting different scattering modes. Although an instrument on the basis of these scattering orders/modes was constructed and demonstrated, the signal quality remained modest to poor, since the absolute scattering intensity is low at these angles and other scattering orders were also significant. The size influence was further complicated by the Gaussian beam effect (e.g. Grehàn et al., 1993), which led to different scattering order mixing for different particle trajectories. Reasonable experimental results were only obtained for particles larger than 50–60μm and for a relatively large relative refractive index.

Recognizing that a conventional phase Doppler instrument will not operate in backscatter, a modified approach has been pursued in the following work. It is based on the volume displacement or time-shift technique (e.g. Albrecht et al., 1993). This technique is only possible with shaped beams and is also the basis of the dual-burst phase Doppler technique (e.g. Onofri et al., 1996) and the pulse-displacement technique (e.g. Pavlovski and Semidetnov, 1991; Hess and Wood, 1993). The essence of this technique lies in the realization that with a shaped beam, each scattering order/mode exhibits its own virtual measurement volume for every detector. The virtual volumes are defined over the scattered intensity as a function of the particle center position for a specific receiver location. These volumes all have the same size as the illuminated volume but are displaced in space. The magnitude of the displacement depends on the scattering order/mode, the receiving location, the relative refractive index and the particle diameter. Thus, if the different scattering orders/modes are identifiable in the received signal at specific detector angles, and the relative refractive index is known, the diameter can be estimated from the time shift between them (see Fig.1).

The main scattering components for the backscatter range, in order of occurrence for $m > 1$ will be: surface wave (long path), reflection, second-order refraction (inner path), second-order refraction (outer path), surface wave (short path). Note that there exist two modes for second-order refraction ($p = 3$). These have been designated $p = 3.1$ (inner path) and $p = 3.2$ (outer path). The origins of these components for a particle traversing a Gaussian beam is shown in Fig. 1.

The relative amplitude between each of the fractional signals will depend on the specific scattering order/mode, and the absolute amplitude scales with the incident power and particle size. The width and shape of each fractional signal is given by the width and shape of the incident beam. Basically, the incident beam is being sampled by the incident points of each scattering order/mode on the surface of the particle and it is being imaged onto the detector. The separation of the fractional signals in time will be determined by the particle size, the relative refractive index and the particle shape. Overlapping of fractional signals from different scattering orders/modes is reduced by keeping the ratio of the particle diameter to the incident beam width large. For practical applications this means a highly focused beam should be used, insuring good separation of the fractional signals even for small particles.

2. SIGNAL CHARACTERISTICS

The remarks of the previous section pertaining to scattering from a single laser beam indicate that the virtual image displacement of each scattering order/mode lies in the plane formed by the axis of the incident beam and the detector direction as seen from the measurement volume region. All fractional signals will therefore only be seen if the particle velocity vector lies in or near this plane. Furthermore, particle sizing using the time-shift technique necessarily requires a measurement of the particle speed. The time shift between scattering orders/modes is measured and this must be related to the volume displacement, hence to the particle size, through speed. Several authors (e.g. Pavlovski and Semidetnov, 1991; Lin et al., 2000) achieved this using two laser beams in a time-of-flight fashion. Alternatively, two beams can be brought to intersection as in laser Doppler systems and the velocity can be measured from the signal modulation frequency. This latter technique will be considered below in investigating various approaches for particle sizing in backscatter.

If a laser Doppler is used for the speed measurement then two incident beams are involved. A separate set of virtual images of the laser beams will exist for each incident beam and each detector. Interference, hence signal modulation and the possibility of a velocity measurement, will only occur if the two virtual images of each of the beams and like scattering order/mode overlap.

The illuminated volume is defined by the e^{-2}-decay of the modulated intensity created by the two incident laser beams without any particle and has an ellipsoidal shape for Gaussian beams. The measurement volumes for each scattering order, which are the virtual images of the illuminated volume, can be defined in the same way by using the amplitude of the receiver signals with respect to the particle position. The centers (maximum received modulated power) are displaced by

$$\mathbf{r}_{max,\approx}^{(p)} = \frac{1}{2}\begin{pmatrix} -(x_1^{(i,p)} + x_2^{(i,p)}) + (z_1^{(i,p)} - z_2^{(i,p)})\tan\Theta/2 \\ -(y_1^{(i,p)} + y_2^{(i,p)}) \\ -(z_1^{(i,p)} + z_2^{(i,p)}) + (x_1^{(i,p)} - x_2^{(i,p)})\cot\Theta/2 \end{pmatrix} \tag{1}$$

from the intersection point of the two beams. The subscripts indicate the two beams (1 for $\Theta/2$ and 2 for $-\Theta/2$). The main axes of the volumes are parallel to the main axis of the illuminated volume. All coordinates of the incident points are linearly dependent on the particle diameter and, therefore, the measurement volume displacement is also linearly dependent on the particle diameter in all three directions.

For intersecting beams, the measurement volumes of a laser Doppler system are also displaced in the z direction, as seen from Eq. (1). Due to the $\cot\Theta/2$-dependence of this displacement, it may well exceed the dimensions of the particle diameter. On the other hand, the glare point distance is approximately linearly dependent on the intersection angle $x_1^{(i,p)} - x_2^{(i,p)} \approx \xi^{(p)}\Theta/2$ for small intersection angles, where the linearity constant $\xi^{(p)}$ depends on particle diameter and scattering mode. These two effects compensate each other and therefore the z position of the measurement volume is only slightly dependent on intersection angle. If the measurement volumes are made long in the z direction, and the glare point distance $x_1^{(i,p)} - x_2^{(i,p)}$ small by choosing a small intersection angle, the probability that a particle which moves in the x direction will pass through all volumes increases. Furthermore, to insure that the measurement volumes for all scattering orders/modes lie in the same plane, the detector or detectors should lie in the same plane as the incident beams, in which case all scattering planes for each beam/detector pair are coincident.

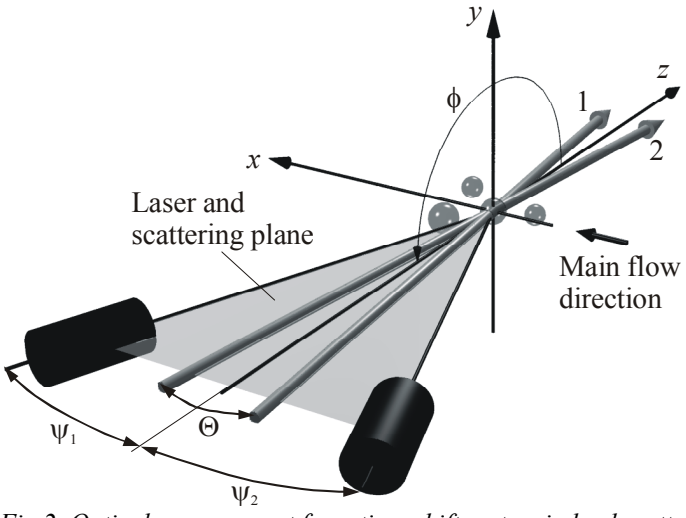

Fig.2. Optical arrangement for a time-shift system in backscatter

For further investigations, an optical arrangement as shown in Fig. 2 has been used, in which two detectors symmetrically placed about the optical axis z are shown. The particles traverse the beam intersection volume along the x axis. This optical arrangement corresponds exactly to the planar backscatter phase Doppler arrangement, in which the detectors lie in the same plane as the incident beams. In keeping with the notation for standard phase Doppler systems, the angle ψ is then known as the elevation angle and the off-axis angle is $\phi = 180\,\text{deg}$. The scattering angles are $\vartheta_s = \psi \pm \Theta/2$. A typical signal received at a single detector of the system shown in Fig. 2

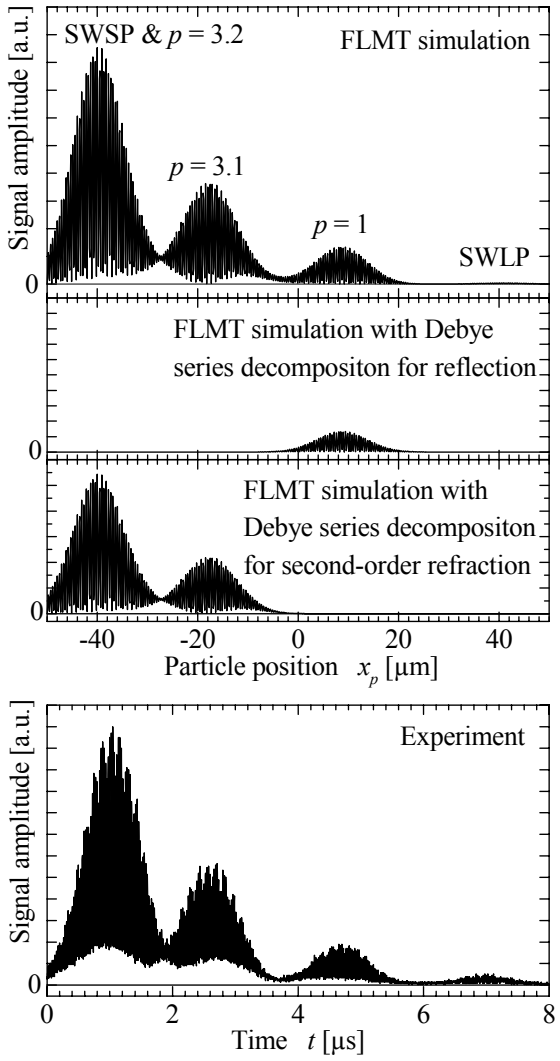

Fig. 3. Signal of a planar phase Doppler system ($\Theta = 7.4$ deg, $\psi = 25$ deg, $\lambda = 514.5$ nm, $d_p = 80$ µm, $d_b = 20$ µm). a) Calculated, b) Measured

is illustrated in Fig. 3, computed using FLMT (Albrecht et al. 1995) and the Debye decomposition of the FLMT (Albrecht et al. 1999) and measured in the laboratory using a transient recorder to record the signal.

For very small intersection angles ($\cos\phi/2 \approx 1$, $\sin\phi/2 \approx \phi/2$) and a planar system, Eq. (1) reduces to

$$\mathbf{r}_{max\approx}^{(p)} = -\frac{1}{2}\begin{pmatrix} x_1^{(i,p)} + x_2^{(i,p)} \\ 0 \\ z_1^{(i,p)} + z_2^{(i,p)} - \xi^{(p)} \end{pmatrix} \qquad (2)$$

The measurement volumes are located in the laser and scattering plane and the x coordinate of the centers of the measurement volumes are between the images of the two laser beams for each scattering order. Therefore, the AC and the DC parts of the signal consist of the same four distinct fractional signals corresponding to the scattering orders/modes shown in Fig. 1. Note that the short path surface wave and the refraction mode $p = 3.2$ overlap almost completely and cannot be individually distinguished.

The separation of the reflected signal fraction from the refractive fraction $p = 3.1$ decreases with decreasing elevation angle. Furthermore, the second-order refraction ($p = 3.2$) increases in amplitude for larger elevation angles. Below about $\psi = 14$ deg ($m = 1.33$), only the $p = 3.1$ mode contributes to second-order refraction. The best fractional signal separation is found for $\psi = 20$ deg.

For a particle trajectory in the x direction and if the relative refractive index of the particle is known, the particle diameter can be measured by measuring the time shift between selected fractional signals. This time shift is transformed into a volume displacement using the particle velocity in the x direction found from the Doppler modulation frequency. For smaller particles the fractional signals overlap increasingly and the estimation of the time shift becomes virtually impossible.

An alternative approach is to use two symmetrically located detectors (see Fig. 2). Assuming the intersection angle Θ to be small, pairs of the beam images will be coincident, so that two sets of measurement volumes will be distinguishable (one for each detector). The situation has been exemplary pictured in Fig. 4a, in which the dominating three measurement volumes for each detector lie along the x axis. Note that the spacing between the volumes depends on particle size, refractive index etc. and that this pictorial is only an example. An important feature is that the volumes appear in reverse sequence for each detector because of the symmetric placement of the detectors about the incident beams, as illustrated in Fig. 4b. This means that the time shift between the two signals from the two receivers can also be measured for smaller particles, because the shifted signals on the two detectors are now separated.

2.1 TRAJECTORY INFLUENCE

The discussion above has presumed that the AC (modulation) and DC parts of the signal are coincident. For small intersection angles Θ this is largely true for particle trajectories in the x-y plane. For trajectory displacements in the z direction however, the AC part will decrease and the DC part will exhibit distinct volumes for each beam. The fractional signals from detector 2 appear in opposite sequence to those from detector 1, because of the asymmetry about the z axis. As examples, signals for two trajectories at $z = 0$ and $z = 160$ µm are shown in Fig 5 for one receiver.

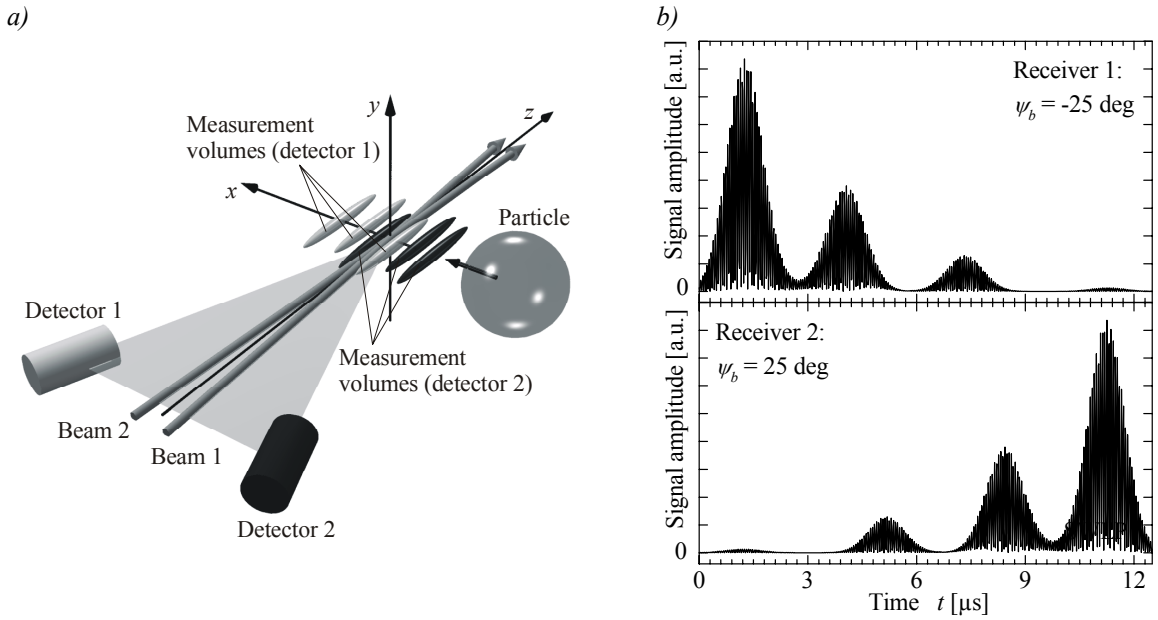

Fig. 4. Planar optical configuration. a) Separated measurement volumes, b) Signals from two receivers ($\Theta = 4$ deg, $\lambda = 514.5$ nm, $d_p = 100$ µm, $d_b = 20$ µm)

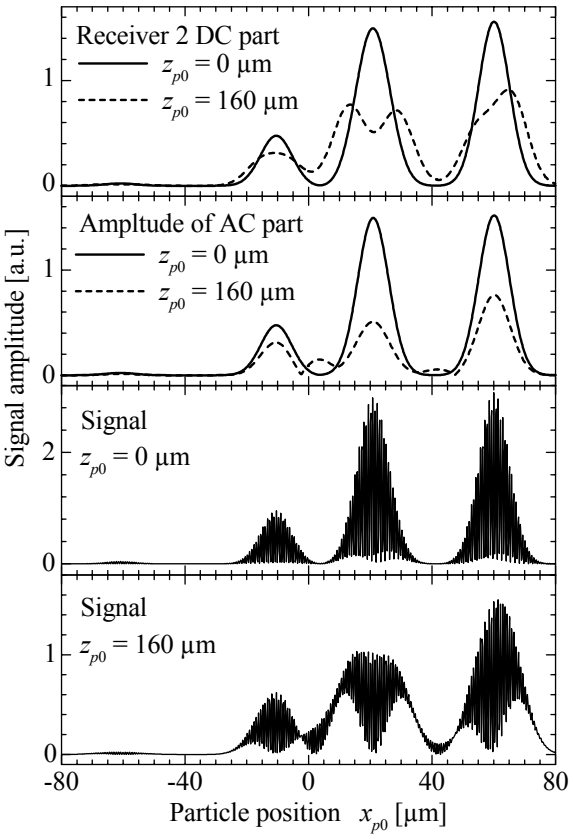

Fig. 5. Signals and DC and AC parts for two particle trajectories parallel to the x axis at $z = 0$ µm and $z = 160$ µm for the configuration from Fig. 4

For trajectories far removed from $z = 0$, the amplitude of the AC part of the signal decreases, although not symmetrically for positive and negative z values. The DC part only decreases insomuch as the incident beams are divergent in the z direction and any z shift of the virtual measurement volume will be accompanied by a slight intensity decrease.

At extreme values of displacement in the z direction, all modulation will disappear and only the DC part will remain, showing two peaks for every scattering order/mode. This corresponds to the particle crossing the two incident laser beams at a non-overlapping position. The particle diameter can be measured by the time shift of the signal maxima. For trajectories parallel to the x axis, the time shift is a direct measure for the measurement volume displacement. In case of oblique trajectories the time shift leads to a systematic error of the volume displacement. For small intersection angles, for receiver locations far from the direct backscatter and for a planar configuration the signal maximum occurs at

$$x_{max\approx}^{(p)} \approx \frac{-\hat{x}^{(p)} + y_{p0} m_y + z_{p0} m_z \Theta/2}{1 + m_y} \qquad (3)$$

By using two detectors the time shift between the signals becomes independent of the particle trajectory intersection with the plane $x = 0$ and independent of the z component of the particle trajectory and depends linearly on particle diameter, as

$$\Delta t_{12}^{(p)} = \frac{\Delta x_{max\approx}^{(p)}}{v_x} = \frac{x_{max\approx,1}^{(p)} - x_{max\approx,2}^{(p)}}{v_x} \approx -\frac{1}{v_x} \frac{\hat{x}_1^{(p)} + \hat{x}_2^{(p)}}{1 + m_y} \qquad (4)$$

The y component must be measured for further corrections with e.g. a two-velocity component laser Doppler system.

2.2 INFLUENCE OF THE REFRACTIVE INDEX

The influence of the refractive index on the time shift signals is illustrated in Fig. 6, showing a simulated detector signal for the values $m = 1.25$ and $m = 1.42$. As the refractive index increases, the position of the $p = 3.1$ fractional signal exhibits a monotonic but non-linear increase of time shift, whereas the reflective fractional signal remains unaffected. The difference in diameter estimated using the time shift of reflection and $p = 3.1$ can be used for determining refractive index. A diameter difference of 5K 6% corresponds to a 0.025 change in *m*. Both the amplitude and position of the $p = 3.2$ fractional signal change with the refractive index, thus also influencing the short path surface wave signal due to the strong overlap. Note that for larger particle diameters, all fractional signal dependencies correspond to values predicted by geometrical optics, at least for small intersection angles ($\Theta < 6\text{K } 7 \text{ deg}$). These dependencies are shown explicitly in Fig.6b calculated with geometrical optics and a Debye decomposition of FLMT results. The surface waves are assumed to be on the circumference of the particle.

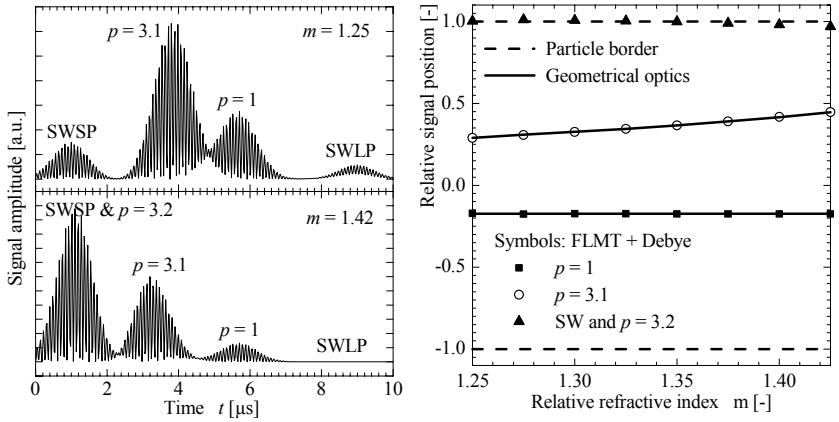

Fig. 6. Change of the signal structure and time shifts due to refractive index changes ($d_p = 80$ µm, $\psi = 20$ deg, $\Theta = 4$ deg, $\lambda = 514.5$ nm, $d_b = 20$ µm)

2.3 INFLUENCE OF SHAPE

It is also interesting to investigate the influence of the non-sphericity on the time shift of fractional signals and this is done using simple oblate and prolate ellipses, as pictured in Fig. 7. The time shift can be expressed as an incident point displacement between –1 and 1, corresponding to the two outer edges of the particle. The surface wave will take the values –1 and 1 and will be of no direct use for detecting non-sphericity. The reflective and refractive signals will be more sensitive. This sensitivity is illustrated in Fig. 8, in which the normalized incident point position is shown as a function of scattering angle and particle aspect ratio a/b. For reflection, an oblate particle exhibits a smaller incident point shift than the spherical particle of diameter $2b$. For $p = 3.1$ the opposite dependency and with an opposite sign is observed. The sensitivity of the $p = 3.1$ fractional signal is also higher. These results have been computed using geometrical optics.

This dependency can be used to estimate non-sphericity for this special case of a planar optical configuration with the major axis of the particle ellipse aligned with the system axis. The sensitivity of such a non-sphericity measurement is shown in Fig. 9 for a receiver angle of $\psi = 20$ deg. The difference in normalized position between the reflection and $p = 3.1$ fractional signal (relative to the –1 and 1 given by the surface waves) yields a rather sensitive estimate for the aspect ratio of ellipticity.

3. PARTICLE SIZING TECHNIQUES USING THE TIME SHIFT

The possibility of using the time-shift technique for particle sizing in backscatter will now be investigated quantitatively for the various scattering orders involved. Size information can be extracted by examining the time shift between signals of like scattering order/mode at different detectors and, using the particle velocity, converting this to a volume displacement. To begin therefore, quantitative expressions for the time shift will be given for reflection and second-order refraction.

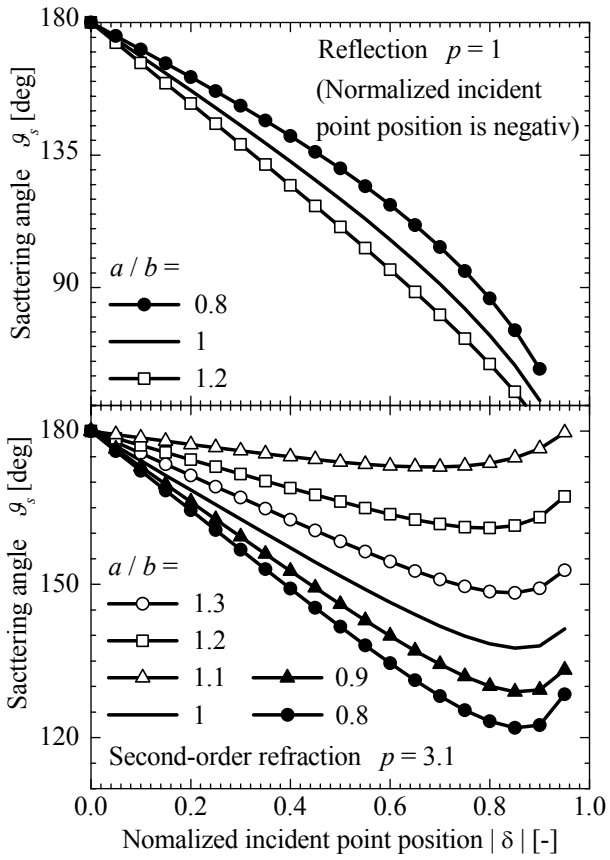

Fig. 8. Normalized between the detector scattering angle and the normalized incident point position for various aspect ratios of ellipticity (m=1.33). p=3.1

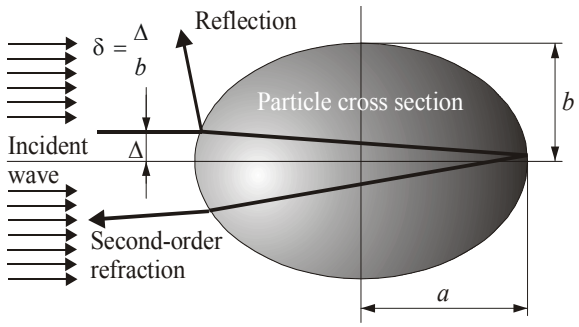

Fig. 7. Geometry of light scattering from an elliptic particle

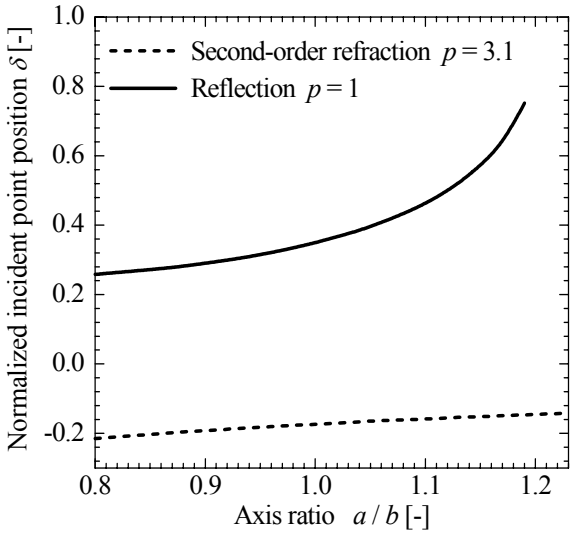

Fig. 9. Relative incident point shift of reflective and refractive (p=3.1) fractional signals as a function o aspect ratio of ellipticity (m=1.33)

General expressions for the position of the incident and glare points can be found in the literature (e.g. Boris 1996). For symmetric receiver locations ($\psi_1 = -\psi_2$) the volume displacement or time shift between the signal maxima for reflection ($p = 1$) and first-order refraction ($p = 2$) can be given as a closed solution for the AC part (Boris 1996). For reflection the time shift for particle trajectories parallel to the *x* direction is

$$\Delta t_{12}^{(p=1)} = \frac{x_{max\approx,1}^{(1)} - x_{max\approx,2}^{(1)}}{v_x} = -\frac{d_p}{2\sqrt{2}v_x}\left(\frac{\cos\psi\cos\phi\tan\vartheta/2 - \sin\psi}{\sqrt{1-\cos\psi\cos\phi\cos\vartheta/2 - \sin\psi\sin\vartheta/2}} - \frac{\cos\psi\cos\phi\tan\vartheta/2 + \sin\psi}{\sqrt{1-\cos\psi\cos\phi\cos\vartheta/2 + \sin\psi\sin\vartheta/2}} \right) \tag{5}$$

where the indexes 1 and 2 indicate the different receivers, as shown in Figs 2 and 4. For the planar configuration ($\phi = 180$ deg) and for the small intersection angles ($\sin\vartheta/2 \approx 0$, $\sin\vartheta/2 \approx 1$) considered here, the incident points of the two beams coincide and the time shift simplifies to

$$\Delta t_{12}^{(1)} = \frac{d_p}{v_x}\sin\frac{\psi}{2}, \quad (\tan\vartheta/2 \approx \vartheta/2,\ \psi >> \vartheta/2,\ \phi = 180 \text{ deg}) \tag{6}$$

A normalized displacement or normalized incident point position independent of particle size can be defined by normalizing Eq (5) with the particle radius $r_p = d_p/2$.

$$\delta^{(p)} = \frac{\Delta^{(p)}}{r_p} \approx \frac{\hat{x}^{(p)}}{r_p}, \qquad \Delta t_{12}^{(p)} \approx \frac{d_p}{v_x}\delta^{(p)} \tag{7}$$

The border of the particle in the x direction then corresponds to the coordinates 1 and –1. For reflection this relation between normalized volume displacement and receiver is given by

$$\delta^{(1)} = \sin\frac{\psi}{2} \tag{8}$$

For second-order refraction the incident point shift will depend additionally on mode ($p = 3.1$ or $p = 3.2$) and on the relative refractive index m . The angular relationship between angle of incident and scattering angle (for the planar configuration the elevation angle can be approximated by the scattering angle, $\psi = \vartheta_S$) is given by

$$\vartheta_s = \pi + 2(\theta_i - 2\theta_t) = \pi + 2\theta_i - 4\arcsin\left(\frac{\sin\theta_i}{m}\right) \tag{9}$$

where the angle of refraction is $\theta_t = \arcsin(\sin\theta_i / m)$.

For a given scattering angle, Eq. (9) must be solved for θ_i iteratively. Solutions are given in Fig. 10 for $m = 1.33$ and $m = 1.5$ in terms of normalized incident point position as a function of the scattering angle. Note that the $p = 3.2$ mode appears only for elevation angles $|\psi| > 15$ deg for the refractive index $m = 1.33$ and that the incident point remains near the periphery of the particle. For larger relative refractive indexes ($m > 1.4$) the situation becomes more complex and the number of fractional signals may even reach the number of the mode p. For instance in Fig 10b a third mode, $p = 3.3$, can be identified. Physically, this means that three different ray paths match to a given detector position, consequently there are three pairs of incident and glare points. Expressions for the relative displacement of higher scattering orders become somewhat more complex but can always be solved numerically using an iteration. For every ray path, e.g. either reflection or second-order refraction in the backscatter region, the resulting time shift is given by

$$\Delta t_{12}^{(p)} = \frac{d_p}{2v_x}\left(\delta_1^{(p)} - \delta_2^{(p)}\right) \tag{10}$$

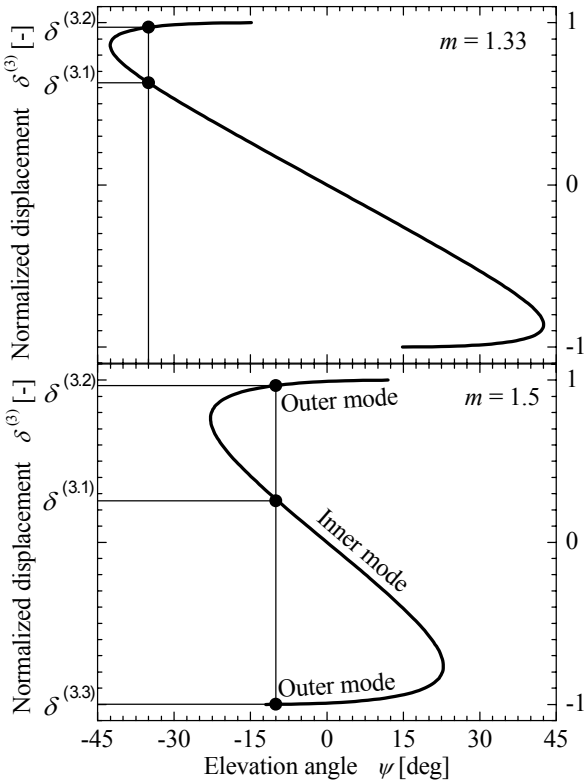

Fig.10. Normalized volume displacement for second-order refraction for refractive indexes of $m = 1.33$ and $m = 1.5$

where δ_1 and δ_2 are the respective relative displacements for detectors 1 and 2. δ_1 and δ_2 are defined by the optical geometry (and relative refractive index). The particle diameter is found by measuring the velocity v_x and the time shift of the considered scattering order/mode and solving Eq. (10) for d_p and for particles moving parallel to the x axis. For other trajectories with $v_y \neq 0$, corrections of the time shift must been made by measuring the v_y velocity component and using Eq. (4).

For particles moving near the x axis and for small intersection angles, the AC and DC parts of the signal will be coincident and the time shift can be measured between the signal maxima of the non-filtered bursts. For trajectories sufficiently displaced along the z axis, or for larger intersection angles, the DC part of each detector signal may exhibit two maxima corresponding to each of the incident beams, as illustrated in Fig. 5 ($z = 160$ mm). The required time shift should be the time between DC maxima from the same beam glare point on each detector. This is somewhat impractical because the DC part is more susceptible to narrow-band noise sources. A more robust measurement can be achieved by using the time shift between AC maxima of the two detectors signals (of like scattering order/mode) as shown in Fig. 5 below.

4 SIGNAL PROCESSING

The accuracy and resolution of the time-shift technique will be in part dependent on the expectation and variance of the estimator used to find the AC part maxima. Note that the estimation procedure must also identify and separate the fractional signals before the estimation of the maxima is performed. A detailed discussion of this procedure can be found in the literature (Nobach, 2002) and will only be briefly reviewed here. The assumption is made in the present study that all fractional signals are always present and that the AC and DC parts are coincident, as in systems with small intersection angles.

Signal processing comprises three steps: signal conditioning, burst separation and parameter estimation. The signal conditioning filters the signal to yield the DC and AC components of the signal. From the sampled AC part, $u_{AC}(t)$, the envelope is extracted using the (complex) analytical signal $u_{AC}(t_i) + j\aleph\{u_{AC}\}(t_i)$, derived using the Hilbert transform $\aleph\{\}$. Two additional low-pass filters are applied to the obtained envelope signal to suppress oscillations and to improve the signal detection. The first filter works in frequency domain. It has a step cut-off frequency to avoid high frequency oscillations. The second filter works in the time domain. It additionally smoothes the signal. Because the peak width is a priori unknown, the burst separation routine is used twice, first with an pre-estimate width with the number N_b of bursts to be detected from the signal and the total time T of the signal. After the first burst separation, the individual peak width estimates are used to derive optimized filter coefficients and to perform the burst separation procedure more accurately.

Each iteration of the procedure yields the arrival time of the highest Gauss peak found in the averaged envelope. This procedure is used repeatedly to obtain the parameters of the N_b bursts. For each detected Gauss peak also the individual width parameter is obtained. With the improved estimate of the Gauss peak width the separation procedure is performed again to obtain better burst separation results.

While the signal conditioning and burst processing is performed on each detector signal, the final processing step determines the time between fractional signals of like scattering order/mode. Therefore, the detector signals are split into N_b subsignals, each separated at their midpoints by the detected arrival times. The subsignals are filled up to N_s samples using zero padding. For each order/mode and detector, the burst signal $u_k(t_i)$ with $k = 1,2,\mathrm{K}\ ,N_b N_d$ is transformed to the spectral domain using the Fourier transform.

$$U_k(f_j) = \sum_{i=1}^{N_s} w_i\, u_k(t_i) \exp(-2\pi \mathrm{j}\, f_j t_i) \qquad (j = 0\mathrm{K}\ N_s - 1\ ,\ \ f_j = j\, f_s / N_s) \tag{11}$$

with the weights

$$w_i = u_{e\,LP}(t_i) u_{DC}(t_i) \tag{12}$$

including both the obtained AC envelope (only low-pass filtered) and the obtained DC part of the input signal. The $N_b N_d$ spectra are multiplied yielding a common spectrum

$$S(f_j) = \prod_{k=1}^{N_b N_d} S_k(f_j) \tag{13}$$

which is used to derive a common Doppler frequency using a second-order parabolic interpolation to the logarithmic spectrum $\log(S(f_i))$ (e.g. Domnick et al., 1988). In a second step the phase spectra are calculated for each burst. Then the individual absolute phases are derived at the detected Doppler frequency using a linear interpolation in the phase spectrum

$$\varphi_k(f_j) = \arg\left(U_k(f_j)\right) \tag{14}$$

Finally, the Doppler frequency of all bursts is used to compute an average particle velocity, hence a volume displacement and particle size.

5 NUMERICAL TEST SIMULATIONS

Particle sizing using the time-shift technique and the optical configuration shown in Fig. 2 has been simulated with the help of signals generated using FLMT. The simulations were performed for the detector elevation angles $\psi_1 = 20$ deg and $\psi_2 = -20$ deg, which represent the best results for all detector positions investigated, and for a measurement volume diameter of $20\ \mu\mathrm{m}$. The results are shown as solid symbols in Fig. 11 for the different fractional signals: surface wave (short path) + second-order refraction ($p = 3.2$) (Fig. 11a), second-

order refraction ($p = 3.1$) (Fig. 11b) and reflection (Fig. 11c). The best results are achieved for the surface wave (short path) + refraction ($p = 3.2$) and the accuracy increases for larger particles. The increased scatter for small particles (for all fractional signals) arises because of the increased overlapping of fractional signals and the low intensity.

A second result is shown in Fig. 11 by the solid line. These results were obtained using geometrical optics to compute the position of the incident points (and glare points) of each order and shows a perfect linear relation. The results for the full signals follow closely the linear curves for isolated orders, with small deviations at very small particle sizes and for refraction ($p = 3.1$).

Finally, Fig. 11 includes results shown by the open symbols. In this case the signal was simulated with the FLMT using only the respective scattering order. This is possible using the Debye series decomposition after the FLMT computations. In this simulation no signal overlapping occurs by definition for the reflected light and the result is a perfect linear relation between size and time shift. Surface waves and the different modes in a single scattering order cannot be calculated separately using the Debye decomposition and therefore they appear all together in the calculations for second-order refraction. For the small particles, the surface wave and $p = 3.1$ fractional signal are mixed. The deviation of the Debye decomposition from the linear relation of geometrical optics in Fig 11b is due to the mixing inside the second-order refraction between surface waves and different second-order modes. The calculations confirm that the scatter in the full-signal results originates from order/mode mixing. Nevertheless, some systematic trends resulting in a non-linear but monotonic diameter/time shift dependency can be predicted and considered in converting the time shift to particle diameter (Fig 11b).

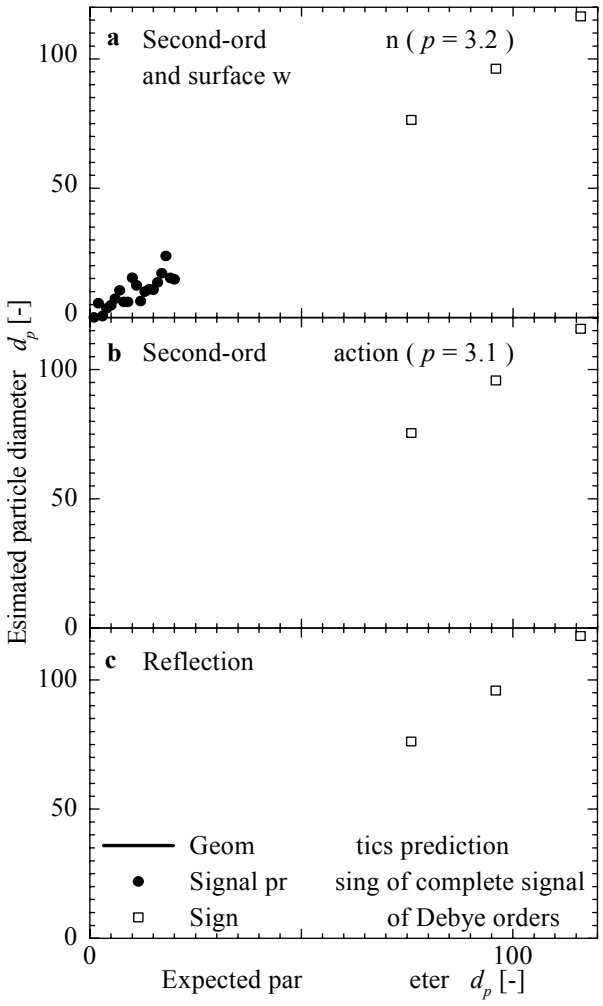

Fig. 11. Particle size estimates from simulated signals using various fractional signals and a 20 µm *measurement volume diameter ($\psi = \pm 20$ deg , $\Theta = 4$ deg , $\lambda = 514.5$ nm , $m = 1.33$). a) Surface wave short path (SPSP) + second-order refraction ($p = 3.2$) , b) Second-order refraction ($p = 3.1$), c) Reflection*

As shown in Eqs. (6), the time shift is a good approximation for size, independent of the diameter of the incident beam. For larger beam diameters, the signals are broader and only a stronger mixing of orders occurs. As expected, the smallest measurable particle size using this technique for the dominant scattering order in backscatter ($p = 3.2$) will be determined by the focused size of the measurement volume ($d_{p,min} = 20$ µm). For the scattering orders with smaller signal amplitudes ($p = 3.1$ and $p = 1$), the limit is already reached at larger diameters ($d_{p,min} = 43$ µm), because the non-dominant scattering orders are overlapping for small particle diameters and the maxima can no longer be identified.

The lower particle size limit can also be reduced by using receiver locations where only one scattering order dominates. This is the case for normal phase Doppler configurations in forward scattering, when using first-order refraction. For such a configuration, the time shift of the dominant order is not disturbed by signals from other scattering orders and the technique is limited by the accuracy of determination of the maximum signal amplitude. This is mainly determined by the signal-to-noise ratio of the signal. The time-shift technique works for particle sizes down to 1/10 of the beam diameter quite well if only one scattering order is used (Boris, 1996). The present paper has considered the time-shift technique only in its backscatter realization.

6 CONCLUSION

The time-shift technique for particle sizing in backscatter has been examined in detail. With the conventional phase Doppler technique particle size measurement in backscatter is only possible in some special cases and therefore very limited.
The imaging of a shaped beam by a particle creates virtual images of the incident beams and virtual measurement volumes for each scattering order. The displacements of these images vary linearly with the particle size and permit a measurement of particle diameter for spherical particles. The dependencies of the displacement on the system parameters has been given for the AC and the DC part of the signal and it has been shown that a planar configuration with a small intersection angle results in useful practical simplifications for particle sizing. For such a configuration the trajectory dependence can be corrected by using a two-velocity component laser Doppler system. Furthermore, such a system offers the determination of refractive index and ellipticity for larger particles in special cases. The scattering orders involved for a backscatter configuration are reflection, second-order refraction and surface waves. A signal processing strategy was presented to separate the different contributions in the resulting detector signal. To demonstrate the backscatter time-shift technique, signals were simulated and processed using the signal processing algorithms introduced. The results show that the time-shift technique works well for particle diameters larger than the beam waist diameter.

ACKNOWLEDGEMENTS

This work has been financially supported by the Deutsche Forschungsgemeinschaft through grant Tr 194/18. Also the company Dantec Dynamics has graciously made equipment available for some of the laboratory investigations.

REFERENCES

Albrecht, Bech, Damaschke, Feleke (1995) Die Berechnung der Streuintensität eines beliebig im Laserstrahl positionierten Teilchens mit Hilfe der zweidimensionalen Fouriertransformation. Optik **100**: 118-124

Albrecht, Borys, Hübner (1993) Generalized theory for simultaneous measurement of particle size and velocity using laser-Doppler- and laser-two-focus methods. Part. Part. Syst. Charact. **10**: 138-145

Albrecht, Borys, Damaschke, Tropea (1999) The imaging properties of particles in laser beams. Meas. Sci. Technol. **10**: 564-574

Borys (1996) Analyse des Amplituden- und Phasenverhaltens von Laser-Doppler-Signalen zur Größenbestimmung sphärischer Teilchen. Dissertation, Shaker-Verlag Aachen

Bultynck (1998) Développements de sondes laser Doppler miniatures pour la mesure de particules dans des écoulemnets réels complexes. Ph.D. Thesis, Université de Rouen

Domnick, Ertl, Tropea (1988) Processing of phase Doppler signals using the cross spectral density function. Proc. 4th Int. Symp. on Appl. of Laser Techn. to Fluid Mechanics. Lisbon Portugal: paper 3.8

Gréhan, Gouesbet, Naqwi, Durst (1993) Particle trajectory effects in phase Doppler systems: computations and experiments. Part Part Syst Charact **10**: 332-338

Hess, Wood (1993) Pulse displacement technique to measure particle size and velocity in high density application. In Adrian et al. (Ed) Laser Tech and Appl in Fluid Mech, Springer Verlag Berlin: 131-144

Hishida, Kobashi, Maeda (1989) Improvement of LDA/PDA using a digital signal processor (DSP). Proc. 3rd Int. Conf. on Laser Anemometry. Swansea UK: paper S2

Lin, Waterman, Lettington (2000) Measurement of droplet velocity, size and refractive index using the pulse displacement technique. Meas Sci Techn **11**: L1-L4

Nobach (2002) Analysis of dual-burst laser Doppler signals. Meas Sci Tech **13**: 33-44

Onofri, Girasole, Gréhan, Gouesbet, Brenn, Domnick, Tropea (1996) Phase-Doppler anemometry with dual burst technique for measurement of refractive index and absorption coefficient simultaneously with size and velocity. Part & Part Syst Charact **13**: 112-123

Pavlovski, Semidetnov (1991) Simultaneous measurement of velocity, size and concentrations for particles moving in two-phase flow. Measurement Technology (Izmeritel'naja Technika) **9**: 40-42 (in Russian)